

THE MECHANICAL BEHAVIOUR OF BRAIN TISSUE: LARGE STRAIN RESPONSE AND CONSTITUTIVE MODELLING

M. Hrapko, J. A. W. van Dommelen, G. W. M. Peters, J. S. H. M. Wismans
Eindhoven University of Technology, Department of Mechanical Engineering
PO Box 513, 5600 MB Eindhoven, The Netherlands

ABSTRACT

The non-linear mechanical behaviour of porcine brain tissue in different deformation modes is determined. An improved method for rotational shear experiments is used, producing an approximately homogeneous strain field and leading to an enhanced accuracy. Results from oscillatory experiments, stress relaxation experiments and constant strain rate experiments are presented. Large deformations at the time scale of loading and the material behaviour during complex loading paths (loading-unloading) is investigated. No significant immediate mechanical damage is observed for these shear deformations. A new differential viscoelastic model is used to describe the non-linear mechanical response of brain tissue. This constitutive model is readily applicable in three-dimensional head models in order to predict the mechanical response of the intra-cranial contents due to an impact.

Keywords: BRAINS, SOFT TISSUES, MODELS, VISCOELASTICITY.

THE HEAD IS OFTEN CONSIDERED as the most critical region of the human body for life-threatening injuries sustained in accidents. The social costs of these accidents were estimated at 160 billions Euro per year in the European Union alone (ETSC, 1999). From 1995 to 2001 an average of 1.4 million cases of traumatic brain injury occurred in the United States each year, of which 20% resulted from motor vehicles accidents (Langlois *et al.*, 2004). In order to develop effective protective measures, a better understanding of the process of injury development in the brain is required.

In the early sixties, the Head Injury Criterion was developed (Versace, 1971) and is still used in most current test standards. However it suffers from a number of drawbacks, one of which is that it is based on linear head acceleration only. Moreover, it does not allow for a distinction between different injury mechanisms. Nowadays, Finite Element (FE) models are being developed, in order to predict the mechanical response of the contents of the head during impact. Current FE head models contain a detailed geometrical description of anatomical components of the head but lack accurate descriptions of the mechanical behaviour of brain tissue. Therefore, brain tissue has been studied with a variety of techniques and a number of constitutive models were proposed. The mechanical behaviour of brain tissue has been mostly tested *in vitro* in shear (Arbogast and Margulies, 1998; Bilston *et al.*, 2001; Brands *et al.*, 2000; Darvish and Crandall, 2001; Donnely and Medige, 1997; Galford and McElhaney, 1970; Nicolle *et al.*, 2004; Peters *et al.*, 1997; Shuck and Advani, 1972; Takhounts *et al.*, 2003; Thibault and Margulies, 1998; Prange and Margulies, 2002), compression (Prange and Margulies, 2002; Estes and McElhaney, 1970; Miller, 1997) and tension (Miller and Chinzei, 2002). Reported properties of brain tissue vary more than an order of magnitude. Several reasons for this scatter may exist, such as differences in testing protocols, different donor species, anisotropy, and the non-homogeneous nature of brain tissue. *Post mortem* times vary from a few hours (Arbogast and Margulies, 1998; Bilston *et al.*, 2001; Brands *et al.*, 2000; Prange and Margulies, 2002) to a few days (Darvish and Crandall, 2001; Donnely and Medige, 1997; Nicolle *et al.*, 2004). Animal brain tissue is frequently used as a substitute for the human brain in experiments to characterize the mechanical behaviour. The main reasons are that animal brains are easily available and can be tested at short *post-mortem* times. In most studies involving human brains, material was obtained from autopsies with the consequence of longer *post mortem* times. The mechanical response of fresh human brain tissue was reported to be approximately 30% stiffer than that of porcine brain tissue (Prange and Margulies, 2002). Similar results have been presented for bovine brain tissue by Takhounts *et al.* (2003).

A number of constitutive models were developed to describe the mechanical behavior of brain tissue. Many researchers use an integral model, often in combination with Ogden hyper-elasticity to describe the viscoelastic behaviour of brain tissue (Darvish and Crandall, 2001; Mendis *et al.*, 1995; Miller, 1999; Nicolle *et al.*, 2004; Prange and Margulies, 2002; Takhounts *et al.*, 2003), and some propose a differential constitutive equation (Bilston *et al.*, 2001; Brands *et al.*, 2004; Donnelly and Medige, 1997). However, these existing models were not validated to describe the influence of non-linear behaviour on different deformation modes and complex loading paths. The ability of a constitutive model to describe this complex mechanical response is crucial for reliable simulations of head injury. Therefore a new model should be developed that is able to describe the response to large deformations in different deformation modes.

This paper presents experimental data on the mechanical response of brain tissue subjected to large deformations for different deformation modes. The occurrence of mechanical damage is investigated by a series of constant shear rate experiments with an increasing strain amplitude. Moreover, results from a series of loading-unloading cycles for different shear rates are presented. Stress relaxation and recovery upon unloading of brain tissue are investigated in both shear and in compression. Based on the experimental results, a new non-linear viscoelastic material model is formulated using a differential framework which is suitable for large deformations. A non-linear elastic mode is used in combination with a number of viscoelastic modes showing shear thinning behaviour. The model is fitted to data obtained from shear experiments and is validated for unconfined compression experiments. It can be expected that if a model is applicable to complex deformation modes of porcine brain tissue, it can also be applied to human brain tissue after determining the appropriate parameters.

METHODS

Porcine brain tissue was tested in both simple shear and in unconfined compression experiments. Porcine brain tissue was chosen as a substitute for human brains because of availability and the possibility to minimize the *post-mortem* time at testing. Fresh halves of porcine brains from 6 month old pigs were obtained from a local slaughterhouse. Immediately after acquisition, it was placed in an ice cooled physiological saline solution to prevent dehydration and to slow down degradation of the tissue. Samples were prepared from the brain halves within 2 hours after sacrifice.

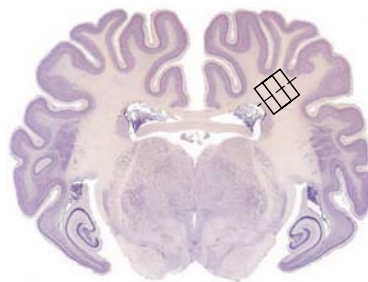


Figure 1: Sample location in a coronal section of a porcine brain.

Fine slices were cut by a Leica VT1000S Vibrating-blade microtome from *corona radiata* region and cylindrically shaped samples were obtained with a cork bore which was applied from the *medial* to the *lateral* side, such that the axis of the cylinder was at 30° from the axis perpendicular to the sagittal plane, see Figure 1. The sample dimensions were $d = 7-10$ mm, $h = 1-3$ mm for shear and $d = 7-9$ mm, $h = 3.5-4.5$ mm for compression tests. Immediately after sample preparation, the samples were placed in a physiological saline solution at 7°C, and subsequently were tested within a 0.5 to 3 hours. All samples were tested within *post-mortem* times ranging from 2.5 to 5 hours.

Shear experiments were performed on an ARES II rotational rheometer with a 10GM FRT transducer in a plate-plate configuration. Waterproof sandpaper (grain size 0.18 mm) was attached to the upper and lower plate to prevent slippage during loading. This configuration was previously shown to be effective by Brands *et al.* (2000). A moist chamber was used to prevent dehydration. The test temperature

was 37°C. An eccentric configuration was used, where the sample was placed at the edge of the plate (Turnhout *et al.*, 2005), with a radius of 25 mm, see Figure 2. The shear stress τ and shear strain γ were then calculated from the measured torque M and angle θ by:

$$\tau = \frac{MR}{2\pi R_1^2 \left(\frac{(R-R_1)^2}{2} + \frac{R_1^2}{8} \right)}, \quad \gamma = \theta \frac{R}{h}, \quad (1)$$

where R is the radius of the plate, R_1 is the sample radius and h is the sample height. It is assumed that the effect of the free boundaries can be neglected while the sample thickness is much smaller than the sample diameter. The advantages of shifting the sample to the edge of the plate are that the measured torque signal is increased and the deformation is more homogenous than in the conventional centered configuration. Consequently, this configuration enables the study of the large strain response of the material.

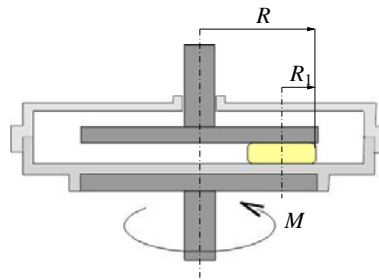


Figure 2: Eccentric configuration for rotational shear experiments.

All shear experiments were preceded by a 10 cycle sinusoidal preconditioning with a frequency of 0.16 Hz and a strain amplitude of 0.01, which was previously determined to be the linear viscoelastic limit by Brands *et al.* (1999) and Nicolle *et al.* (2004). This was confirmed by strain sweep measurements on the current setup. Thereafter, a dynamic sinusoidal strain was conducted with a amplitude of 0.01 and the frequency ranging from 0.04 to 16 Hz. For each frequency, the storage modulus G' and the loss modulus G'' were determined from cycle 2-6. Subsequently, the same sample was tested in either a series of stress relaxation experiments, constant shear rate experiments for different shear rates, or constant shear rate experiments with an increasing strain amplitude. The latter experiments were designed to investigate any potential damaging effect of a previous strain history on the immediate mechanical response. These loading-unloading tests were conducted with a constant shear rate of 1 s^{-1} and the strain was incrementally increased from 0.01 up to 0.5, see Figure 3a. After each loading-unloading cycle the sample was left to recover at zero strain for at least 10 times the loading time. Thereafter, in the next cycle, the strain amplitude was increased. In another test sequence (Figure 3b), loading-unloading cycles with a strain amplitude of 0.15 were conducted with the constant shear rate per cycle increasing from 0.01 s^{-1} to 1 s^{-1} . Between two cycles, the sample was left to recover for at least 10 times the loading time. The stress relaxation experiments were composed of a series of ramp-and-hold tests at different strain levels, see Figure 3c. The strain rate during the loading phase was 1 s^{-1} and the strain was held for 10 s during which the relaxation of the material was recorded and the relaxation modulus $G(t) = \tau(t)/\gamma$ was computed. Then, the strain was released with a constant strain rate of 1 s^{-1} and the sample was left to recover for a period of at least 100 s during which the tissue response was recorded as well. The test was repeated for different strain levels where the strains were chosen to be: 0.01, 0.05, 0.1, 0.15, respectively.

Unconfined compression experiments were performed on an MTS 831.10 servo-hydraulic testing system with a 10N force transducer (MTS 661.09B-20 axial, dynamic, fatigue-rated load cell). Teflon tape was attached to the upper and the lower plate of the compression setup in order to minimize friction effects. During testing, the temperature was 22°C and the samples were kept hydrated by regularly applying saline solution. The samples were tested in a series of stress relaxation experiments which were composed of ramp-and-hold tests at same strain level. The linear strain rate during the loading phase

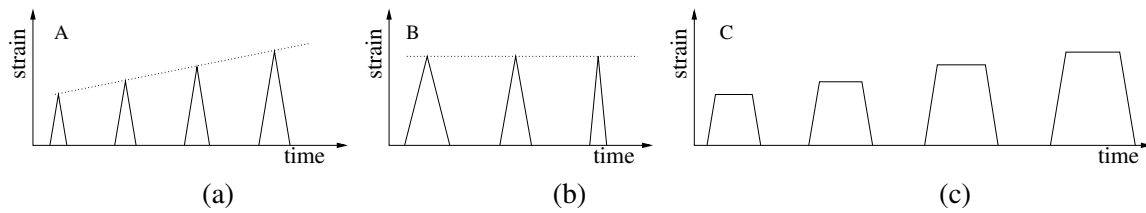


Figure 3: Schematic illustration of test sequences for large strain shear experiments.

was 1 s^{-1} and the strain, which is defined as $\varepsilon = \lambda - 1$, with λ the stretch ratio, was held for 10 s at an amplitude of -0.1 or -0.11 , respectively. Then the strain was released with the same strain rate as in the loading phase and the sample was left to recover at zero strain for at least 10 times the loading time. Subsequently, the same samples were tested in shear within one hour according to the previously described test sequence C.

RESULTS

Dynamic frequency sweep results of 7 samples in terms of storage modulus G' and loss modulus G'' with an average standard deviation of 28% are shown in the Figure 4. This deviation may be caused by differences between the samples and the brains and by local anisotropy. The results compare well with those from Brands *et al.* (2000).

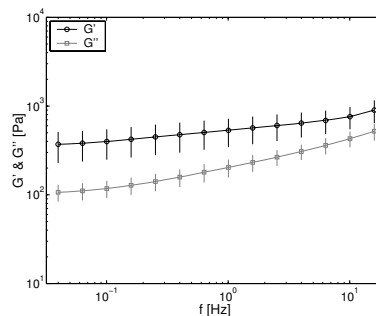


Figure 4: Storage modulus and loss modulus obtained in dynamic frequency sweep experiments.

Results from constant shear rate experiments with an increasing strain amplitude are presented for a representative sample in Figure 5a and b. In Figure 5b, the 0.01 strain limit for linear behaviour is clearly visible in the beginning of each loading part. There was no yield, or failure visible for the tested strain range. By comparing different loading-unloading cycles it can be observed that there is no significant immediate mechanical damage affecting the stress-strain behaviour due to previous shear deformations occurring at the time scale of the experiment. For strains larger than 0.25, the stress-strain curve starts to decrease slightly which is caused by incomplete recovery after the unloading phase, although the time for recovery was more than 10 times the loading and unloading time which can be attributed to non-linearities in the material behaviour. However, the results obtained prove that measurements up to a strain of 0.2 and shear rate of 1 s^{-1} are reproducible for short time scales. In Figure 5c, results from constant shear rate experiments at different shear rates are shown. These tests were performed to show the non-linear strain rate sensitivity of brain tissue. The strain of 0.15 was chosen according to the results of test sequence A, where it was found that below a strain of 0.2 the material fully recovers. From these results it can be observed that also in the non-linear range, the stress as a function of strain is strain rate dependent and that the response stiffens with increasing strain rate. The linear strain limit seems to be the same for all strain rates.

In Figure 6 results are shown from stress relaxations experiments on two samples. During the loading phase the stress response weakens above the linear viscoelastic strain limit and is identical for each stress relaxation test, Figure 6b. This confirms the conclusion from the constant strain rate tests that

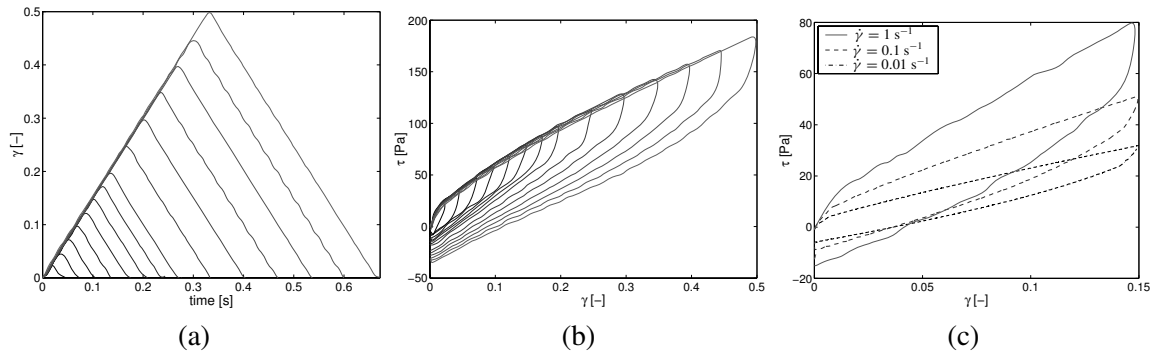


Figure 5: (a), (b) Results from constant shear rate experiment with increasing strain amplitude (test sequence A). (a) Applied shear strain with reproducible strain rate, (b) stress-strain response. (c) Stress-strain response obtained during constant shear rate experiments at different shear rates (test sequence B).

there is no immediate mechanical damage for these strain levels. During stress relaxation the relaxation modulus does not reach a plateau value within the time range allowed, see Figure 6a. This is supported by the findings of all other researchers who performed stress relaxation experiments. As is seen from Figure 6c, the observed relaxation modulus decreases as a function of applied strain, where the difference becomes smaller for larger strains. This represents the true material behaviour and is in contrast with results of the other researchers using rotational rheometer with a concentric configuration. Here an approximately homogenous shear field was obtained by placing the samples at the edge of the plate. Similar behaviour was observed in simple shear measurements on a translational shearing device by Prange and Margulies (2002). Stress relaxation curves for different strain values are nearly parallel.

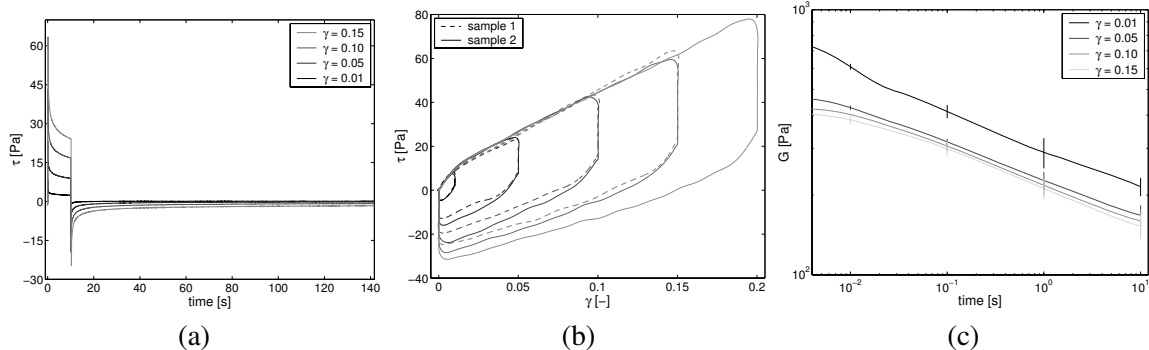


Figure 6: Results from stress relaxation experiments in shear (test sequence C). (a) Stress vs. time for one sample; (b) Stress-strain behaviour for two samples; (c) average stress relaxation modulus from the two samples with a mean deviation of 5.5%.

For strains higher than 0.05 the tissue behaves differently in the loading and unloading parts of stress relaxation. The stress response in the unloading part of the relaxation test with 0.2 shear strain was approximately 24% smaller than in the loading part. After unloading the sample recovers completely for strains in the linear region. For strains above the linear viscoelastic limit, the sample does not recover completely, although the time for recovery was more than 10 times the relaxation time.

Results from compression of two samples are presented in Figure 7a, where the superimposed wavy behaviour is due to inertia effects which are caused by the experimental setup. In Figure 7b, the normalized relaxation modulus is shown for both shear and compression tests. This normalized relaxation modulus is defined as the relaxation modulus ($G(t)$ or $E(t)$, respectively) divided by the maximum relaxation modulus observed immediately upon applying the sample deformation. The (*normalized*) relaxation modulus is also called here the (*normalized*) step response since it is compared with relaxation

after the reversed step which is called here the (*normalized*) reverse step response. From these measurements it can be observed that brain tissue shows a higher rate of relaxation in compression than in shear. This effect is less pronounced for the recovery part of the stress relaxation test.

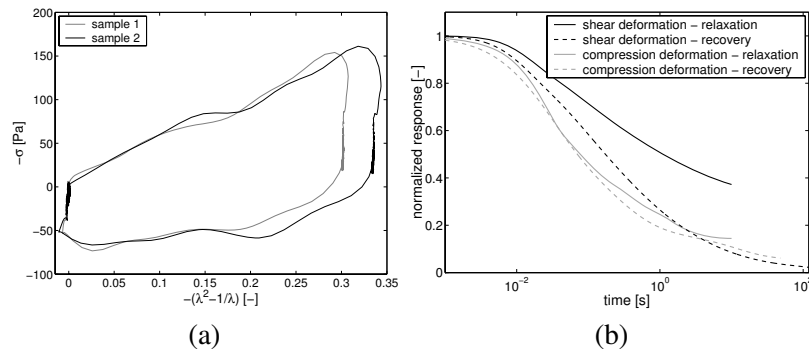


Figure 7: (a) Results from stress relaxation experiments in compression. (b) Comparison of normalized response during relaxation and recovery from shear and compression stress relaxation tests at a strain of 0.1.

It should be noted that during these tests the temperature was not the same. Arbogast *et al.* (1997) did not find any effect of temperature on the viscoelastic response of brain tissue. A temperature sweep on the shear rheometer showed only a linear decrease of the relaxation modulus with temperature, which was also observed by Brands *et al.* (2000) and Peters *et al.* (1997). Therefore the temperature difference has no influence on the normalized relaxation modulus.

CONSTITUTIVE MODEL

A parallel arrangement of a number of viscoelastic modes and a non-linear elastic mode is chosen to model the mechanical behavior of brain tissue. The total Cauchy stress tensor $\boldsymbol{\sigma}$ is written as the summation of these contributions:

$$\boldsymbol{\sigma} = -p\mathbf{I} + \boldsymbol{\sigma}_e^d + \sum_{i=1}^N \boldsymbol{\sigma}_{ve_i}^d, \quad (2)$$

where the superscript “d” indicates that the extra stress is deviatoric and N represents the number of viscoelastic modes. In the current considerations, the material is assumed to be incompressible. A general differential framework is used to describe the viscoelastic modes (Peters and Baaijens, 1997). It is based on a multiplicative decomposition of the deformation gradient tensor \mathbf{F} into an elastic part and an inelastic part for each mode i , denoted by the subscripts “e” and “p”, respectively:

$$\mathbf{F} = \mathbf{F}_e \cdot \mathbf{F}_p, \quad (3)$$

where for clarity, the subscript i has been omitted. This decomposition considers the concept of a local intermediate stress-free state which results from instantaneous elastic unloading of the current configuration. Accordingly, the velocity gradient tensor $\mathbf{L} = \dot{\mathbf{F}} \cdot \mathbf{F}^{-1}$ is decomposed as:

$$\mathbf{L} = \mathbf{L}_e + \mathbf{L}_p \quad \text{with} \quad \mathbf{L}_e = \dot{\mathbf{F}}_e \cdot \mathbf{F}_e^{-1} \quad \text{and} \quad \mathbf{L}_p = \mathbf{F}_e \cdot \dot{\mathbf{F}}_p \cdot \mathbf{F}_p^{-1} \cdot \mathbf{F}_e^{-1}. \quad (4)$$

Furthermore, the inelastic deformations are chosen to be spin-free: $\boldsymbol{\Omega}_p = \frac{1}{2}(\mathbf{L}_p - \mathbf{L}_p^T) = \mathbf{O}$. Based on the kinematics of this framework, the following evolution equation for the inelastic deformations can be derived:

$$\dot{\mathbf{C}}_p = \mathbf{F}^T \cdot \mathbf{B}_e^{-1} \cdot [(\mathbf{L} - \mathbf{L}_e) \cdot \mathbf{B}_e + \mathbf{B}_e \cdot (\mathbf{L}^T - \mathbf{L}_e^T)] \cdot \mathbf{B}_e^{-1} \cdot \mathbf{F}, \quad (5)$$

where \mathbf{C}_p and \mathbf{B}_e represent the inelastic right Cauchy–Green deformation tensor and the elastic Finger tensor, respectively. An explicit integration procedure is used for this evolution equation. In each viscoelastic mode of the model, the deviatoric part of the extra stress tensor is assumed to be given by a

relationship of the form $\sigma_{ve}^d(\mathbf{F}_e)$. Based on the relaxation behaviour of brain tissue, a two-parameter Mooney-Rivlin model is chosen, which reduces to a simple neo-Hookean in shear and provides an extra parameter to adapt the model to different deformation modes. This model can alternatively be written as:

$$W = \frac{1}{2}G_{ve} [aI_{e_1} + (1-a)I_{e_2} - 3] \quad \rightarrow \quad \sigma_{ve}^d = G_{ve} [a\mathbf{B}_e^d - (1-a)(\mathbf{B}_e^{-1})^d], \quad (6)$$

with I_{e_i} the invariants of \mathbf{B}_e . The inelastic flow in a mode is driven by the deviatoric elastic stress and is given by the associated flow rule:

$$\mathbf{D}_p = \frac{1}{2\eta(\tau)} \sigma_{ve}^d, \quad (7)$$

where the viscosity parameter η may depend on the equivalent stress measure $\tau = \sqrt{\frac{1}{2}\sigma^d : \sigma^d}$, where σ^d represents the deviatoric part of the total stress experienced by the material.

Experience with many other materials has indicated that non-linearity often originates from the inelastic part. Here, the Ellis model is chosen to describe the stress-dependence of the viscosity:

$$\eta = \eta_\infty + \frac{\eta_0 - \eta_\infty}{1 + \left(\frac{\tau}{\tau_0}\right)^{n-1}}. \quad (8)$$

This model considers a powerlaw dependence, with a plateau value η_0 for small stress levels and a value of η_∞ for infinite values of τ . The latter is chosen here as $\eta_\infty = k\eta_0$.

A non-linear equilibrium mode is added to the viscoelastic modes. This mode is described by a Mooney-Rivlin-type model, modified with a damping function:

$$\sigma_e^d = 2\frac{\partial W}{\partial I_1}\mathbf{B}^d - 2\frac{\partial W}{\partial I_2}(\mathbf{B}^{-1})^d, \quad (9)$$

with $W = W(I_1, I_2)$ the strain energy function. The shape of the partial derivatives of the strain energy function is chosen based on the non-linear strain-dependence of the equilibrated response to the shear relaxation tests:

$$W = G_e \left\{ -\frac{(1-A)}{C^2} [(Cx + 1) \exp(-Cx) - 1] + \frac{1}{2}Ax^2 \right\}, \quad (10)$$

with

$$x = \sqrt{bI_1 + (1-b)I_2 - 3}. \quad (11)$$

With this strain energy function, the constitutive relation for the equilibrium mode can be written as:

$$\sigma_e^d = G_e \left[(1-A) \exp\left(-C\sqrt{bI_1 + (1-b)I_2 - 3}\right) + A \right] [b\mathbf{B}^d - (1-b)(\mathbf{B}^{-1})^d]. \quad (12)$$

The parameter b distinguishes between the contribution of the first and the second invariant of \mathbf{B} to the strain energy and cannot be determined in shear experiments. Therefore, this parameter can, without other than shear experimental data, be set to $b = 1$.

MODEL APPLICATION

The model described in the previous section was fitted by a least-squares error method to the loading and relaxation part of a shear stress relaxation test (for parameters see Table 1). The coefficient τ_0 was chosen as the stress corresponding to the linear viscoelastic strain limit. The parameters A , C and G_e in the elastic spring contribution were fitted to the damping function obtained from the end points of the relaxation part of the stress relaxation experiments. Then, the viscoelastic parameters G_i , λ_i , and the viscous parameters n , k were fitted to the loading and the relaxation part of the stress relaxation data for the test with a strain of 0.2.

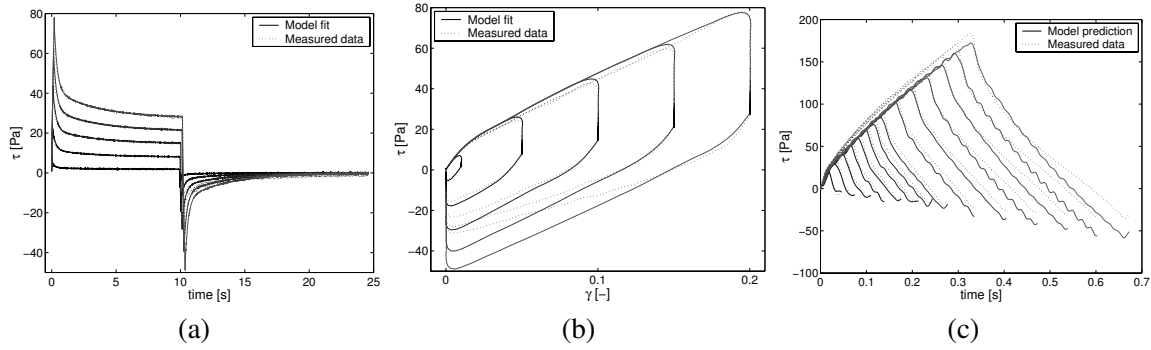


Figure 8: (a), (b) Model fitted to a stress relaxation experiment in shear. (c) Model prediction for constant shear rate experiments on a different sample.

From Figures 8a and 8b, can be seen that model was fitted well to the loading and relaxation part and is able to predict the response of these stress relaxation tests. The unloading and recovery parts are less well described and therefore the viscous parts of the viscoelastic modes require further improvement. The determined parameter set was validated for the loading and unloading part of constant shear rate experiments on a different sample, see Figure 8c. The model predicts the response of the loading-unloading cycles reasonably well, with a maximum deviation of 12.4%. The coefficients a and b should be fitted to the data from compression measurements. However, by adjusting these parameters, no good description of the compression results can be obtained. In the model prediction of the compression results in Figure 9, the parameters a and b are chosen to equal 1. The model prediction of the loading phase of the compression test using the model that was fitted to shear experiments is reasonably good. In order to predict the stress relaxation in compression further model improvement is required. For example, a pressure dependence of the viscosity function may lead to a proper distinction between the shear and compression response.

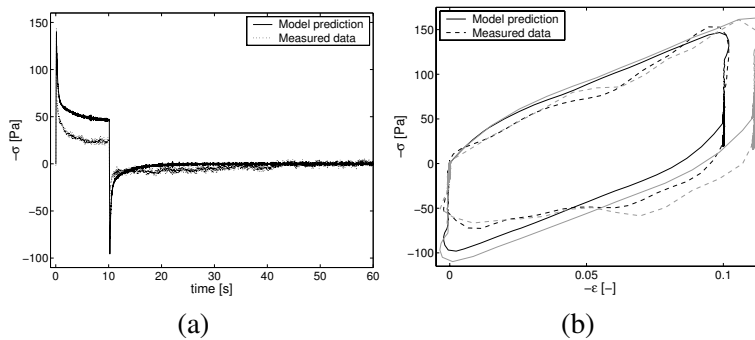


Figure 9: Model prediction for the stress relaxation in the compression experiment.

| Elastic and viscous parameters | Viscoelastic parameters | |
|--------------------------------|--------------------------|---------------------|
| $G_e = 182.9 \text{ Pa}$ | $G_1 = 835.5 \text{ Pa}$ | $\lambda_1 = 0.012$ |
| $A = 0.73$ | $G_2 = 231.2 \text{ Pa}$ | $\lambda_2 = 0.35$ |
| $C = 15.6$ | $G_3 = 67.1 \text{ Pa}$ | $\lambda_3 = 4.62$ |
| $n = 1.65$ | $G_4 = 3.61 \text{ Pa}$ | $\lambda_4 = 12.1$ |
| $\tau_0 = 9.7 \text{ Pa}$ | $G_5 = 2.79 \text{ Pa}$ | $\lambda_5 = 54.3$ |
| $k = 0.39$ | | |

Table 1: Fitted model parameters.

DISCUSSION AND CONCLUSIONS

In this paper, the *in vitro* large strain mechanical response of porcine brain tissue in shear and compression tests is investigated. With the improved method for rotational shear experiments, using an eccentric sample placement, local anisotropy can be studied. The occurrence of slippage during measurements was previously investigated by Brands *et al.* (2000) on a similar experimental setup and was found to be absent. Also Bilston *et al.* (2001) used sandpaper (150 grade) and reported no slip for strains up to 20 with similar shear rates to ours. Therefore, it is assumed that no slip was present.

Results from dynamic frequency sweep tests show that the samples stiffen with increasing frequency. No cross point for the storage and loss modulus was found in the frequency range used in these measurements. When comparing the linear viscoelastic parameters with results presented by other authors, the values obtained in this study are in the lower part of the range reported in literature and are comparable with the data presented by Arbogast and Margulies (1997, 1998), Brands *et al.* (2000), Peters *et al.* (1997) and Thibault and Margulies (1998).

The occurrence of mechanical damage, defined as an immediate change of the mechanical response due to previous deformation, was investigated by a sequence of loading-unloading cycles. It was concluded that no immediate damage was observed up to a strain of 0.45. Moreover, it was found that for strains larger than 0.2 the sample did not recover completely after the loading-unloading cycle which indicates a non-linearity of the material behaviour. No maximum in the stress-strain response was found in the constant strain rate measurements even though the samples were tested up to a strain of 0.5. This is in agreement with the findings of Arbogast *et al.* (1995), Bilston *et al.* (2001), and Donnelly and Medige (1997).

A decrease of the relaxation modulus with increasing strain was found in the stress relaxation measurements, which is in agreement with Arbogast *et al.* (1995), Bilston *et al.* (2001), Brands *et al.* (2000), Nicolle *et al.* (2004), Peters *et al.* (1997) and Prange and Margulies (2002). This effect was decreasing with strain level for strains higher than linear viscoelastic limit which differs from the results of Brands *et al.* (2000) and Nicolle *et al.* (2004). This difference may be attributed to the non-homogeneous shear field in case of a conventional centered geometry. It was found that for strains in the nonlinear regime, the sample did not recover completely. The mechanical response during recovery was not reported by other researchers. Comparable sequences of tests were performed by Prange and Margulies (2002) who reported no structural changes in the tissue during stress relaxation experiments up to a strain of 0.5 and shear rates of 8.33 s^{-1} .

It is for the first time that results from shear as well as compression stress relaxation experiments of brain tissue are presented. During compression experiments the samples showed a higher rate of relaxation than during shear tests. The response during the constant strain rate loading part of the compression test seems to be nearly identical to that obtained in shear and is in between reported data of Miller (1997) and Prange and Margulies (2002).

A differential constitutive model was formulated and subsequently fitted to the presented experimental data. The model predicts the response during the loading phase and the relaxation phase well but is not able to correctly predict the behaviour during unloading and recovery. Therefore, further improvements to the non-linearity of the model are required. In addition, in order to describe the response to compressive loading, further model refinement is needed. It was found that using Mooney-Rivlin type models for the elastic part did not provide the possibility to capture the differences between shear and compression deformation modes.

This constitutive model is readily applicable in three-dimensional head models, where the non-linear nature of the constitutive behaviour may have significant consequences for the predicted mechanical response (Brands *et al.*, 2002). Furthermore, also local anisotropy and regional differences, which are not considered in this study, can strongly affect stress and strain fields in impact situations. Finally, in addition to the compressive response, also the tensile behaviour should be investigated.

ACKNOWLEDGEMENTS

This work was supported by the European integrated project APROSYS.

REFERENCES

- Arbogast, K. B. and Margulies, S. S. (1997). Regional differences in mechanical properties of the porcine central nervous system. *Proc. of the 41st Stapp Car Crash Conference*, SAE 973336:293–300.
- Arbogast, K. B. and Margulies, S. S. (1998). Material characterization of the brainstem from oscillatory shear tests. *Journal of Biomechanics*, 31(9):801–807.
- Arbogast, K. B., Meaney, D. F., and Thibault, L. E. (1995). Biomechanical characterization of the constitutive relationship for the brainstem. *Proc. of the 39th Stapp Car Crash Conference*, SAE 952716:153–159.
- Arbogast, K. B., Thibault, K. L., Pinheiro, B. S., Winey, K. I., and Margulies, S. S. (1997). A high-frequency shear device for testing soft biological tissues. *Journal of Biomechanics*, 30(7):775–759.
- Bilston, L. E., Liu, Z., and Phan-Thien, N. (2001). Large strain behavior of brain tissue in shear: Some experimental data and differential constitutive model. *Biorheology*, 38:335–345.
- Brands, D. W. A., Bovendeerd, P. H. M., Peters, G. W. M., and Wismans, J. S. H. M. (2000). The large shear strain dynamic behavior of in-vitro porcine brain tissue and the silicone gel model material. *Proc. of the 44th Stapp Car Crash Conference*, 2000-01-SC17:249–260.
- Brands, D. W. A., Bovendeerd, P. H. M., Peters, G. W. M., Wismans, J. S. H. M., Paas, M. H. J. W., and van Bree, J. L. M. J. (1999). Comparison of the dynamic behavior of the brain tissue and two model materials. *Proc. of the 43rd Stapp Car Crash Conference*, 99SC21:57–64.
- Brands, D. W. A., Bovendeerd, P. H. M., and Wismans, J. S. H. M. (2002). On the potential importance of non-linear viscoelastic material modelling for numerical prediction of the tissue response: test and application. *Stapp Car Crash Journal*, 46:103–121.
- Brands, D. W. A., Peters, G. W. M., and Bovendeerd, P. H. M. (2004). Design and numerical implementation of a 3-d non-linear viscoelastic constitutive model for brain tissue during impact. *Journal of Biomechanics*, 37:127–134.
- Darvish, K. K. and Crandall, J. R. (2001). Nonlinear viscoelastic effects in oscillatory shear deformation of brain tissue. *Mechanical Engineering & Physics*, 23:633–645.
- Donnelly, B. R. and Medige, J. (1997). Shear properties of human brain tissue. *Journal of Biomechanical Engineering*, 119:423–432.
- Estes, M. S. and McElhaney, J. H. (1970). Response of brain tissue of compressive loading. *An ASME Publication*, 70-BHF-13:4.
- ETSC (1999). Exposure data for travel risk assessment. *European Transport Safety Council, Brussels, Belgium*.
- Galford, J. E. and McElhaney, J. H. (1970). A viscoelastic study of scalp, brain, and dura. *Journal of Biomechanics*, 3:211–221.
- Langlois, J. A., Rutland-Brown, W., and Thomas, K. E. (2004). Traumatic brain injury in the united states: Emergency department visits, hospitalizations, and deaths. *Centers for Disease Control and Prevention, National Center for Injury Prevention and Control, Atlanta (GA)*.
- Mendis, K. K., Stalnaker, R. L., and Advani, S. H. (1995). A constitutive relationship for large deformation finite element modeling of brain tissue. *Journal of Biomechanical Engineering*, 117:279–285.
- Miller, K. (1997). Constitutive modeling of brain tissue: Experiment and theory. *Journal of Biomechanics*, 30:1115–1121.

- Miller, K. (1999). Constitutive model of brain tissue suitable for finite element analysis of surgical procedures. *Journal of Biomechanics*, 32:531–537.
- Miller, K. and Chinzei, K. (2002). Mechanical properties of brain tissue in tension. *Journal of Biomechanics*, 35:483–490.
- Nicolle, S., Lounis, M., and Willinger, R. (2004). Shear properties of brain tissue over a frequency range relevant for automotive impact situations: New experimental results. *Proc. of the 48th Stapp Car Crash Journal*, 48:1–20.
- Peters, G. W. M. and Baaijens, F. (1997). Modelling of non-isothermal viscoelastic flows. *J Non-Newtonian Fluid Mech.*, 68:205–224.
- Peters, G. W. M., Meulman, J. H., and Sauren, A. H. J. (1997). The applicability of the time/temperature superposition principle to brain tissue. *Biorheology*, 34(2):127–138.
- Prange, M. T. and Margulies, S. S. (2002). Regional, directional, and age-dependent properties of the brain undergoing large deformation. *Journal of Biomechanical Engineering*, 124:244–252.
- Shuck, L. Z. and Advani, S. H. (1972). Rheological response of human brain tissue in shear. *Journal of Basic Engineering*, 94:905–911.
- Takhounts, E. G., Crandall, J. R., and Darvish, K. K. (2003). On the importance of nonlinearity of brain tissue under large deformations. *Stapp Car Crash Journal*, 47(03S-67R):14.
- Thibault, K. L. and Margulies, S. S. (1998). Age-dependent material properties of the porcine cerebrum: Effect on pediatric inertial head injury criteria. *Journal of Biomechanics*, 31:1119–1126.
- Turnhout, M. V., Oomens, C., Peters, G., and Stekelenburg, A. (accepted 2005). Passive transverse mechanical properties as a function of temperature of rat skeletal muscle in vitro. *Biorheology*.
- Versace, J. (1971). A review of the severity index. *Proceeding of 15th Stapp Car Crash Conference, Coronado, CA, SAE 710881:771–796*.